


Deep Generative Models for 3D Medical Image Synthesis


Paul Friedrich
Yannik Frisch
Philippe C. Cattin


Abstract Deep generative modeling has emerged as a powerful tool for synthesizing realistic medical images, driving advances in medical image analysis, disease diagnosis, and treatment planning. This chapter explores various deep generative models for 3D medical image synthesis, with a focus on Variational Autoencoders (VAEs), Generative Adversarial Networks (GANs), and Denoising Diffusion Models (DDMs). We discuss the fundamental principles, recent advances, as well as strengths and weaknesses of these models and examine their applications in clinically relevant problems, including unconditional and conditional generation tasks like image-to-image translation and image reconstruction. We additionally review commonly used evaluation metrics for assessing image fidelity, diversity, utility, and privacy and provide an overview of current challenges in the field.

1 Introduction

Medical imaging plays a critical role in diagnosing, monitoring, and treating disease by providing unique structural, functional, and metabolic information about the human body. While natural images usually capture data in two dimensions, medical practice often requires the acquisition of three-dimensional volumes like Magnetic Resonance Imaging (MRI), Computed Tomography (CT), or Positron Emission

Paul Friedrich 
Department of Biomedical Engineering, University of Basel, Hegenheimermattweg 167b, 4123 Allschwil, Switzerland e-mail: paul.friedrich@unibas.ch

Yannik Frisch 
Graphical-Interactive Systems, Technical University Darmstadt, Fraunhoferstr. 5, 64283 Darmstadt, Germany e-mail: yannik.frisch@gris.tu-darmstadt.de

Philippe C. Cattin 
Department of Biomedical Engineering, University of Basel, Hegenheimermattweg 167b, 4123 Allschwil, Switzerland e-mail: philippe.cattin@unibas.ch

Tomography (PET) scans. Acquiring these volumetric scans can be time-consuming, costly, limited by scanner availability, and in the case of CT and PET scans, expose patients to harmful radiation. In addition, privacy and ethical concerns make it difficult to share medical data. Together, these factors limit the availability of large-scale medical image datasets for scientific studies, deep learning in medical image analysis, or physician training.

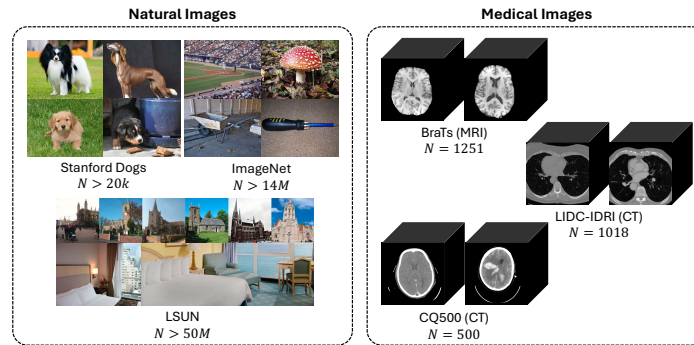


Fig. 1 Differences between natural and medical images. Natural 2D images [22, 60, 134] are widely available in large-scale datasets, as they can easily be scraped from the internet. In contrast, 3D medical data [4, 5, 17, 53, 85] is scarce due to the high cost of acquisition, as well as ethical and privacy concerns.

Driven by advances in generating synthetic natural images, the application of deep generative models to medical images has emerged as a promising solution to address data scarcity and enable various medical image analysis tasks [29, 33, 35, 65]. However, the three-dimensionality and distinct distribution characteristics of medical images, shown in Figure 1, present unique challenges for image synthesis, requiring a careful adaptation of standard methods [122]. This chapter explores the basics of popular image generation models such as Variational Autoencoders (VAEs), Generative Adversarial Networks (GANs), and Denoising Diffusion Models (DDMs), discusses the advantages and disadvantages of each model type, reviews their applications in various medical imaging tasks, and takes a look at common evaluation metrics for assessing model performance.

1.1 Deep Generative Models

Generative models are a class of machine learning models that aim to learn the underlying distribution p_{data} of some input data x to (1) generate new samples from that same distribution or (2) assign probability values to existing samples, allowing for certain downstream tasks. In Deep Generative Models (DGMs), this probability density estimation task is solved using deep neural networks that either

explicitly model the distribution p_{model} or parameterize a model that can sample from p_{model} without explicitly estimating it. This general principle of finding a model that accurately represents the underlying data distribution of some input data x is shown in Figure 2.

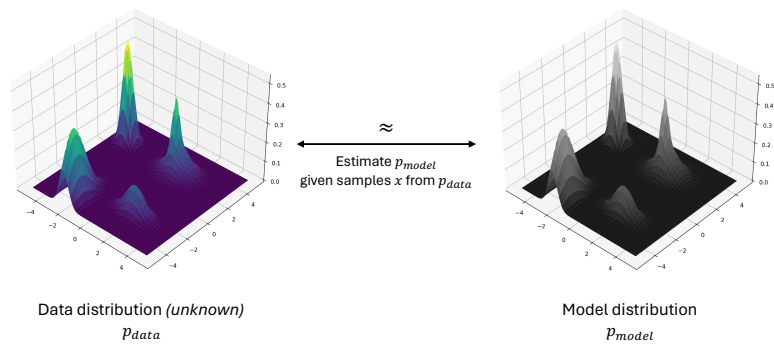


Fig. 2 The basic principle of generative modeling. Using data from the data distribution p_{data} , we try to find a model p_{model} that closely follows this distribution. We can then use this model to generate new samples that resemble the original data distribution.

In recent years, deep generative modeling has been applied to various data modalities, including text [115], audio [87], shapes [78], and images [39], using models such as Restricted Boltzmann Machines [31], Normalizing Flows [97], Variational Autoencoders [64], Generative Adversarial Networks [39], and Denoising Diffusion Models [48, 106].

2 Background on Deep Generative Models

The following section focuses on deep generative modeling of 3D medical images $x \in \mathbb{R}^{D \times H \times W}$ with VAEs, GANs and DDMs, as these models are widely used in medical image computing. We will briefly describe the basic principle of each model, provide insights into their training objectives, and discuss the advantages and disadvantages of the different networks.

2.1 Variational Autoencoders

The basic principle of VAEs [64, 98] builds on that of standard autoencoders. Both encode an input x , e.g. a 3D medical image, into a low-dimensional latent representation $z = E(x)$ using an encoder network E . The original image $x' = D(z)$ is then reconstructed from this representation z using a decoder network D . VAEs,

however, differ in the way they parameterize this latent representation. Instead of directly encoding the image x into a single vector z , they encode it into the parameters of a normal distribution by designing the encoder in a way to predict the mean $\mu = E_{\mu}(x)$ and variance $\sigma^2 = E_{\sigma}(x)$ of that distribution. The latent representation z can then be drawn from $\mathcal{N}(\mu, \sigma^2)$. As backpropagating through this stochastic part would be impossible, VAEs apply a reparameterization trick and instead sample an auxiliary variable $\epsilon \sim \mathcal{N}(0, I)$ to define $z = \mu + \sigma^2 \odot \epsilon$. In addition, VAEs apply a KL-divergence regularization term to this latent distribution to make it close to a standard normal distribution. This allows generating new samples by drawing $z \sim \mathcal{N}(0, I)$ and passing it through the trained decoder network. This general setup is shown in Figure 3. Combining these two principles, VAEs can be trained by

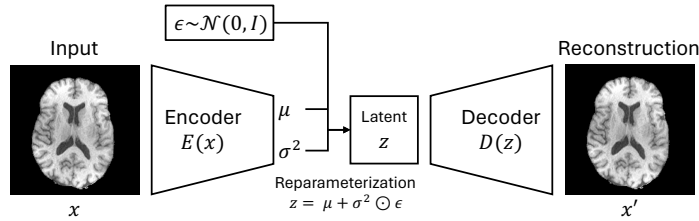


Fig. 3 The basic principle of Variational Autoencoders. An input image x is encoded into a KL regularized latent representation $z = E(x)$ and is subsequently reconstructed as $x' = D(z)$. By minimizing the reconstruction error, as well as the KL-divergence between the latent and a standard normal distribution, the model learns to generate new data and encode data in a meaningful way.

minimizing the reconstruction error between input and reconstructed image, as well as by applying the KL-divergence regularization term to the latent representation, which results in the following training objective:

$$\mathcal{L}_{VAE} = \|x - D(E(x))\|_2^2 - D_{KL}(\mathcal{N}(E_{\mu}(x), E_{\sigma}(x)) \| \mathcal{N}(0, I)). \quad (1)$$

This objective maximizes the evidence lower bound (ELBO) on the log-likelihood of the data. The model, therefore, learns to generate new data and compress data into a meaningful latent representation. While VAEs have a relatively short inference time and are known for their ability to produce diverse images, they suffer from poor sample quality and often produce blurry images [128]. To overcome this problem, variations such as Vector Quantized VAEs (VQ-VAEs) [114] were proposed that map to a discrete learned instead of a continuous static latent distribution. Another commonly used variant is VQ-GAN [28], which combines the VQ-VAE concept with the adversarial training of GANs, another DGM that we will discuss in the next section.

2.2 Generative Adversarial Networks

In recent years, GANs [39] have successfully been used to generate medical images, and form the basis of many applications in the medical field. Unlike most other generative models, GANs don't explicitly model the underlying data distribution in terms of a probability density function but take a different approach by implicitly modeling the distribution through a process of adversarial training. GANs are trained

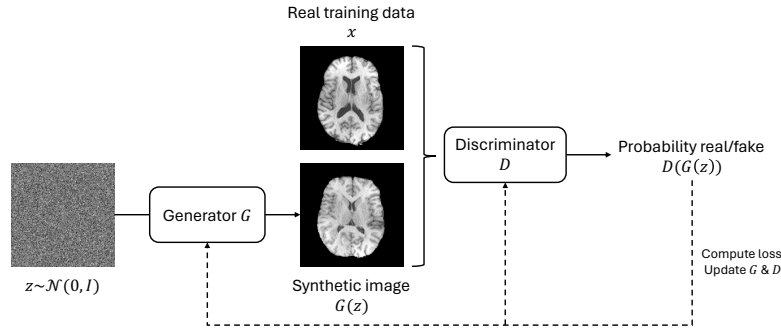


Fig. 4 The basic principle of Generative Adversarial Networks. The generator G and the discriminator D play an adversarial game against each other, where the generator tries to synthesize realistic images that the discriminator cannot distinguish from the real training data.

following a two-player min-max game shown in Figure 4, and generally consist of two networks: the Generator $G(z)$ that aims to generate realistic fake samples from random noise $z \sim \mathcal{N}(0, I)$ and the Discriminator $D(x)$ that tries to distinguish real and fake samples by solving a classification task. Both networks are iteratively optimized using the following training objective:

$$\min_G \max_D \mathcal{L}_{GAN}(D, G) = \mathbb{E}_{x \sim p_{data}} [\log D(x)] + \mathbb{E}_{z \sim \mathcal{N}(0, I)} [\log(1 - D(G(z)))] \quad (2)$$

Intuitively, the generator aims to produce increasingly realistic fake data to fool the discriminator, while the discriminator tries to get better at distinguishing real data from fake data. While GANs have demonstrated impressive image generation capabilities [11, 58], they often suffer from problems such as training instabilities and convergence problems. These issues can be caused by a mismatch between the capacity of the generator and the discriminator or an overconfident discriminator that makes it difficult for the generator to learn and optimize its parameters. Another common problem is mode collapse, where the generator learns to output limited variations of samples by ignoring certain modes of the data distribution. To overcome these problems, various GAN modifications that apply improved training techniques, regularization strategies, or loss modifications have been introduced. Those include Wasserstein GAN (WGAN)[2], WGAN with Gradient Penalty (WGAN-GP) [43], Spectral Normalization GAN (SNGAN) [86], or Least Squares GAN (LSGAN)

[81]. These adaptations have successfully reduced GAN-related problems but do not completely eliminate them.

2.3 Denoising Diffusion Models

Denoising Diffusion Models [48, 106] are latent variable models that sample from a distribution by reversing a defined diffusion process. This *diffusion* or *forward process* progressively perturbs the input data with Gaussian noise and maps the data distribution to a simple prior, namely a standard normal distribution. To generate new samples, we aim to learn the *reverse process*, which maps from this prior to the data distribution. New samples are generated by drawing random noise from the prior and passing it through the reverse process. This general principle is shown in Figure 5. The diffusion process consists of T timesteps and can be described as

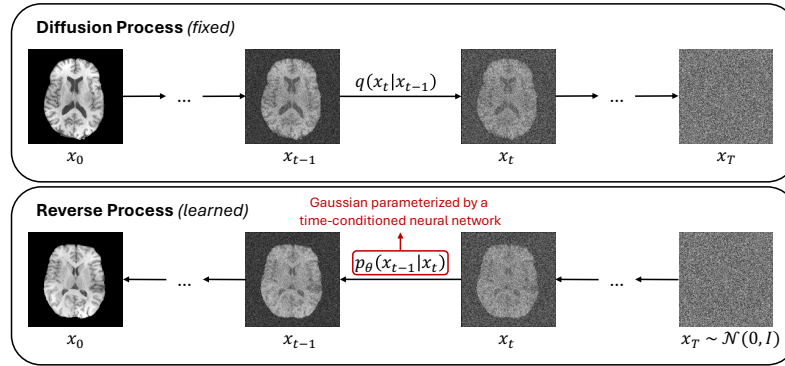


Fig. 5 The basic principle of Denoising Diffusion Models. The diffusion model consists of two main components: a fixed *diffusion process* that gradually perturbs input data with Gaussian noise and maps the data distribution to a simple prior, and a learned *reverse process* with each transition being a Gaussian parameterized by a time-conditioned neural network.

a Markov chain, with each transition being a Gaussian that follows a predefined variance schedule β_1, \dots, β_T :

$$q(x_{1:T}|x_0) := \prod_{t=1}^T q(x_t|x_{t-1}), \quad \text{with} \quad q(x_t|x_{t-1}) := \mathcal{N}(\sqrt{1 - \beta_t}x_{t-1}, \beta_t I). \quad (3)$$

The reverse process can also be described as a Markov chain with learned Gaussian transition kernels, starting at a simple prior distribution $p(x_T) = \mathcal{N}(0, I)$:

$$p_\theta(x_{0:T}) := \prod_{t=1}^T p_\theta(x_{t-1}|x_t), \quad \text{with} \quad p_\theta(x_{t-1}|x_t) := \mathcal{N}(\mu_\theta(x_t, t), \Sigma_\theta(x_t, t)). \quad (4)$$

While $\Sigma_\theta(x_t, t)$ is often fixed to the forward process variances β_t , $\mu_\theta(x_t, t)$ is usually estimated by a time-conditioned neural network. This network is trained by minimizing the variational lower bound of the negative log-likelihood. Following a reparameterization trick [48], we can configure the network to predict the noise $\epsilon_\theta(x_t, t)$ to be removed from a corrupted sample x_t and simplify the training objective to an MSE loss, with $\alpha_t = 1 - \beta_t$, $\bar{\alpha}_t = \prod_{s=1}^t \alpha_s$, and $\epsilon \sim \mathcal{N}(0, I)$:

$$\mathcal{L}_{simple} = \|\epsilon - \epsilon_\theta(x_t, t)\|_2^2, \quad \text{where} \quad x_t = \sqrt{\bar{\alpha}_t}x_0 + \sqrt{1 - \bar{\alpha}_t}\epsilon. \quad (5)$$

Given a trained network $\epsilon_\theta(x_t, t)$ and a randomly drawn starting point $x_T \sim \mathcal{N}(0, I)$, we can iteratively produce a new sample by applying the following equation T times:

$$x_{t-1} = \frac{1}{\sqrt{\alpha_t}} \left(x_t - \frac{1 - \alpha_t}{\sqrt{1 - \bar{\alpha}_t}} \epsilon_\theta(x_t, t) \right) + \sigma_t \epsilon \quad (6)$$

While diffusion models have demonstrated impressive image generation capabilities [23], their iterative nature requires multiple network evaluations for generating a single sample, making them slow and resource-intensive. To speed up this sampling process, several adaptations have been introduced, such as the Denoising Diffusion Implicit Model (DDIM) [107], which formulates a deterministic non-Markovian process to sample with fewer steps, different knowledge distillation methods, such as consistency distillation [108], or combinations of different approaches, such as adversarial training of the denoising network, as proposed in DDGAN [128].

2.3.1 Latent Diffusion Models

To reduce the computational complexity of standard DDMs, Latent Diffusion Models (LDMs) [99] have been introduced. While LDMs share the same fundamental principle as standard denoising diffusion models, they operate on a learned, more compact latent representation of the data rather than directly on the images. Training LDMs begins with training an autoencoder, such as VQ-GAN [28], to generate a meaningful low-dimensional latent representation of the data. Subsequently, the diffusion model is trained on this latent representation z instead of the original high-dimensional data x , resulting in a more computationally efficient approach. This principle is illustrated in Figure 6. To generate new samples, the reverse diffusion process is applied starting from random noise $z_T \sim \mathcal{N}(0, I)$ in the latent space, producing a synthetic latent representation z_0 . This latent representation is then decoded back into the image space using the trained decoder. Although LDMs effectively reduce the computational complexity of training and sampling from denoising diffusion models, they depend on a well-performing autoencoder. Training

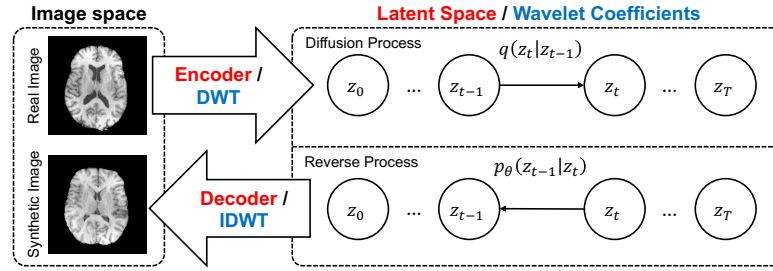


Fig. 6 The basic principle of Latent Diffusion Models (red) and Wavelet Diffusion Models (blue).

such an autoencoder for high-resolution medical volumes is challenging itself and often constrained by computational resources.

2.3.2 Wavelet Diffusion Models

Wavelet diffusion models (WDMs) [33, 92], shown in Figure 6, are a promising alternative to LDMs. While both approaches share a similar idea, wavelet diffusion models take a different approach to spatial dimensionality reduction by applying Discrete Wavelet Transform (DWT). This approach is learning-free in the sense that it does not require a pre-trained autoencoder. The diffusion model then operates on the wavelet coefficients z of the images. To generate new images, WDMs start with random noise $z_T \sim \mathcal{N}(0, I)$ and apply the reverse diffusion process to produce synthetic wavelet coefficients z_0 . These coefficients can then be transformed back to the image space using Inverse Discrete Wavelet Transform (IDWT). As WDMs do not rely on an autoencoder network, they have an even smaller memory footprint than LDMs, which is particularly important in 3D medical image synthesis tasks that are typically constrained by the available GPU memory.

3 Applications in Medical Image Computing

The following section provides an overview of DGMs in 3D medical image synthesis. Starting with the fundamental task of unconditional image generation, followed by a discussion of conditional image generation tasks, including image-to-image translation and image reconstruction. It is important to note that this only covers a subset of potential applications of DGMs in medicine. Additional tasks, such as image registration [61], classification [72], segmentation [125, 127], anomaly detection [103, 124], and image inpainting [26, 34] can also be addressed using generative networks.

3.1 Unconditional Image Generation

Unconditional image generation involves the synthesis of new images without any specific condition and simply demonstrates the ability of a generative model to learn the underlying distribution of some given training data. These models can be applied to augment datasets with synthetic images [131] or improve downstream applications fairness under distribution shifts [66]. Unconditional image generation is commonly used to demonstrate the performance of novel architectures, which serve as a foundation for developing methods for conditional generation tasks. An overview of publications that present unconditional 3D medical image synthesis models is given in Table 1, where we provide information on the synthesized image modality, the image resolution, the public datasets used for training, as well as the network architecture.

Although VAEs are widely used for modeling 2D medical images, their application to unconditional 3D image generation remains relatively unexplored. Volokitin et al. [116] used 2D slice VAEs to model high-resolution 3D brain MR images by combining a VAE with a Gaussian model that allows for sampling coherent stacks of latent codes that decode into a meaningful volume. Kapoor et al. [57] took a different approach by transforming a reference MRI with multi-scale morphological transformations predicted by a 3D VAE.

GAN-based approaches have been extensively explored for 3D medical image synthesis, with early applications successfully modeling brain MR images. Kwon et al. [68] and Segato et al. [104] adapted the α -GAN framework [80] for this purpose, while Hong et al. [49] presented a 3D version of StyleGAN [58]. While these early approaches were constrained to relatively low resolutions, Chong et al. [18] were the first to scale GAN-based methods to higher resolutions by applying morphological transformations and texture changes to reference volumes. Sun et al. [110] reached similar resolutions following a hierarchical approach that first generates a low-resolution image and then performs a learned upsampling operation. Liu et al. [77] relied on pretraining 2D models and inflating the 2D convolutions [14] to improve the performance of 3D models.

Dorjsembe et al. [24] were the first to adapt the standard Denoising Diffusion Probabilistic Model (DDPM) [48] for modeling 3D medical data, achieving promising results on a brain MR image generation task. Despite their success, the computational complexity and long sampling times associated with simple 3D adaptations posed significant challenges. Peng et al. [91] explored a 2.5D approach that models 3D volumes by iteratively predicting 2D slices conditioned on their predecessors and generates new volumes in an autoregressive fashion. Further advances were made by Pinaya et al. [93] and Khader et al. [59], who applied latent diffusion models to high-resolution 3D data, effectively reducing the computational complexity and sampling times. However, training the required 3D autoencoder on high-resolution volumes remains a challenging problem and is usually constrained by the available hardware. Friedrich et al. [33] proposed applying discrete wavelet transform for spatial dimensionality reduction. This allowed scaling 3D diffusion models to higher resolutions

Table 1 Overview of publications on unconditional 3D medical image synthesis models, the modality of the generated data, public datasets used for training, the maximum image resolution reported in the paper, as well as the utilized network architecture.

Study	Model	Modality	Dataset(s)	Resolution	Network(s)
Volokitin et al. (2020) [116]	VAE	MRI	HCP	$256 \times 256 \times 256$	2D Slice-VAEs
Kapoor et al. (2023) [57]	VAE	MRI	ADNI	$80 \times 96 \times 80$	3D VAE
Kwon et al. (2019) [68]	GAN	MRI	ADNI, BRATS, ATLAS	$64 \times 64 \times 64$	3D α -WGAN-GP
Segato et al. (2020) [104]	GAN	MRI	ADNI	$64 \times 64 \times 64$	3D α -GAN
Granstedt et al. (2021) [41]	GAN	MRI	fastMRI	$256 \times 256 \times 16$	3D GAN
Hong et al. (2021) [49]	GAN	MRI	ADNI, ABIDE, ADHD2000, HABS, GSP, MCIC, OASIS, PPMI	$80 \times 96 \times 112$	3D StyleGAN
Chong et al. (2021) [18]	GAN	MRI	HCP	$256 \times 256 \times 256$	3D WGAN-GP + 2D pix2pixGAN
Bergen et al. (2022) [9]	GAN	PET	HECKTOR	$64 \times 64 \times 32$	2D TGAN
Mensing et al. (2022) [84]	GAN	MRI	German National Cohort	$160 \times 160 \times 128$	3D cGAN (FastGAN)
Sun et al. (2022) [110]	GAN	MRI, CT	GSP, COPDGene	$256 \times 256 \times 256$	3D HA-GAN
Liu et al. (2023) [77]	GAN	MRI	COCA, ADNI	$64 \times 64 \times 64$	2D StyleGAN2 + 3D StyleGAN2
Kim et al. (2024) [62]	GAN	MRI, CT	HCP, CT-ORG	$128 \times 128 \times 128$	3D WGAN-GP
Dorjsembe et al. (2022) [24]	DDM	MRI	ICTS	$128 \times 128 \times 128$	3D DDPM
Pinaya et al. (2022) [93]	LDM	MRI	UK Biobank	$160 \times 224 \times 160$	3D VAE + 3D DDPM/DDIM
Peng et al. (2023) [91]	DDM	MRI	ADNI, UCSF, SRI International	$128 \times 128 \times 128$	2.5D DDPM
Khader et al. (2023) [59]	LDM	MRI, CT	DUKE, MR-Net, ADNI, LIDC-IDRI	$128 \times 128 \times 128$	3D VQ-GAN + 3D DDPM
Friedrich et al. (2024) [33]	WDM	MRI, CT	BRATS, LIDC-IDRI	$256 \times 256 \times 256$	3D WDM (DDPM)

without training an autoencoder and outperformed latent diffusion models on brain MRI and lung CT generation tasks.

3.2 Image-to-Image Translation

Multimodal data plays an important role in medical imaging. However, its accessibility is often limited by challenges such as acquisition time and cost, scanner availability, and the risk of additional radiation exposure. To address these limitations, image-to-image translation models aim to generate synthetic images y of a missing modality given an available source modality image x . In other words, these

models try to find a mapping function $F : X \rightarrow Y$ that maps from the source domain X to the target domain Y , such that $y = F(x)$. This problem can be addressed in a paired setting, where training samples $\{x_i, y_i\}_{i=1}^N$ consist of corresponding images $x_i \in X$ and $y_i \in Y$ from the different domains, or in an unpaired setting, where the training data $\{x_i | x_i \in X\}_{i=1}^N$ and $\{y_j | y_j \in Y\}_{j=1}^M$ consists of unrelated samples, requiring different training strategies. Table 2 provides an overview of publications on image-to-image translation models for 3D medical images. The table includes information on the translation task, the public datasets used for training, whether the approaches utilized paired or unpaired data, as well as the used network architecture.

Table 2 Overview of publications on 3D image-to-image translation frameworks, the translation modalities, public datasets used for training (– for private data), the type of translated data (paired vs. unpaired), as well as the utilized network architecture.

Study	Model	Modality	Dataset(s)	Type	Network(s)
Hu et al. (2022) [50]	VAE	MRI \leftrightarrow MRI	BRATS	Paired	2D Spatial-VAE
Wei et al. (2019) [121]	GAN	MRI \rightarrow PET	–	Paired	3D cGAN
Uzunova et al. (2020) [112]	GAN	CT \leftrightarrow CT, MRI \leftrightarrow MRI	COPDGene, BRATS	Unpaired	3D cGAN
Hu et al. (2021) [51]	GAN	MRI \leftrightarrow PET, MRI \leftrightarrow CT	ADNI, TCIA	Paired	3D BMGAN
Lan et al. (2021) [70]	GAN	MRI \rightarrow PET	ADNI	Paired	3D SC-GAN
Lin et al. (2021) [76]	GAN	MRI \leftrightarrow PET	ADNI	Paired	3D RevGAN
Sikka et al. (2021) [105]	GAN	MRI \rightarrow PET	ADNI	Paired	3D cGAN
Zhao et al. (2021) [138]	GAN	MRI \leftrightarrow MRI	BRATS	Paired	3D CycleGAN
Zhang et al. (2022) [136]	GAN	MRI \rightarrow PET	ADNI	Paired	3D BPGAN
Bazangani et al. (2022) [8]	GAN	PET \rightarrow MRI	ADNI	Paired	3D E-GAN
Kalantar et al. (2023) [55]	GAN	CT \leftrightarrow CT	NCCID	Unpaired	3D CycleGAN
Poonkodi et al. (2023) [94]	GAN	PET \leftrightarrow CT, PET \leftrightarrow PET, MRI \leftrightarrow MRI	Lung-PET- CT-Dx	Unpaired	3D CSGAN
Wang et al. (2024) [117]	GAN	MRI \rightarrow PET	–	Paired	3D ViT-GAN
Durrer et al. (2023) [27]	DDM	MRI \leftrightarrow MRI	–	Paired	2D DDPM
Graf et al. (2023) [40]	DDM	MRI \rightarrow CT	MRSpineSeg	Paired	3D DDIM
Pan et al. (2023) [90]	DDM	MRI \leftrightarrow MRI	BRATS	Paired	3D DDPM
Zhu et al. (2023) [140]	LDM	MRI \leftrightarrow MRI	RIRE	Paired	2D VAE + 2.5D DDPM/DDIM
Zhu et al. (2024) [139]	LDM	Mask \rightarrow MRI, Mask \rightarrow CT	BRATS, AbdomenCT- 1K	Paired	2D VAE + 2.5D DDIM
Kim et al. (2024) [63]	LDM	MRI \leftrightarrow MRI	BRATS, IXI	Paired	3D VQ-GAN + 3D DDPM
Dorjsembe et al. (2024) [25]	DDM	Mask \rightarrow MRI	BRATS	Paired	3D DDPM
Pan et al. (2024) [89]	DDM	MRI \rightarrow CT	–	Paired	3D DDPM
Li et al. (2024) [74]	DDM	MRI \rightarrow PET	ADNI	Paired	2.5D DDPM

A common task in medical image computing is MRI-to-MRI translation (e.g. T1 \leftrightarrow T2, or 1.5T \leftrightarrow 3T), which serves several purposes. First, it provides physicians with different contrasts of the images to aid in diagnosis and treatment planning. Second, it can improve the performance of downstream applications such as segmentation tasks by providing the segmentation model with multiple MRI contrasts to work with. Finally, it allows for harmonizing scans from different MR scanners,

reducing potential biases in the acquired datasets. These problems have been tackled using VAE-based[51], GAN-based [94, 112, 138] or DDM/LDM-based approaches [27, 62, 140] and have also been addressed in scientific challenges like the MICCAI 2023 Brain MR Image Synthesis for Tumor Segmentation challenge [6].

Another application involves generating CT or PET scans from MR images. This enables downstream tasks to be performed on the target modalities without exposing patients to additional CT or PET imaging radiation. For example, Graf et al. [40] performed MRI-to-CT translation to enable segmentation networks trained on CT scans to be applied to MR images. Recently, the SynthRAD challenge [52], which aims to provide tools for radiation-free radiotherapy planning by translating MR images to CT scans, has drawn significant attention to this task and highlights the need for well-performing image-to-image translation methods. The task of MRI-to-CT/PET translation has been tackled using different GAN-based [51, 70, 76, 105, 119, 121, 136] and DDM-based approaches [74, 89].

Medical image-to-image translation is not only used to translate between different contrasts and modalities but has also been adapted for other tasks, such as anomaly localization, by transforming pathological images into their pseudo-healthy versions [103, 123, 124]. These approaches, however, have not yet been explored on 3D images.

Image-to-image translation models have proven to be valuable tools for assisting physicians and enabling certain downstream tasks. However, these models have inherent limitations and should not be applied naively. Image-to-image translation models rely on the information present in the input image and the learned prior knowledge of the target modality. This means that if specific clinically relevant details are missing or poorly represented in the source image, they cannot be accurately generated or inferred in the translated image. In addition, these models tend to hallucinate realistic-looking features that do not necessarily correspond to the actual anatomical structures that should be present in the image. As a result, a translated image may contain elements that falsely appear normal or pathological, leading to potential misdiagnosis if naively assumed to be correct.

3.3 Image Reconstruction

Reconstructing high-quality images from sparsely sampled or partial measurements is important in speeding up existing medical imaging tools such as CT, PET, or MRI, reducing examination times, harmful radiation exposure to patients, and acquisition costs of these methods. Typical medical image reconstruction tasks include, but are not limited to:

- **Sparse-view computed tomography (SV-CT):** Aims to reconstruct images from a limited number of X-ray projections.
- **Limited-angle computed tomography (LA-CT):** Aims to reconstruct images from X-ray projections taken over a limited angular range. Similar to SV-CT, the

number of projections is reduced compared to standard CT, but the acquisition angle is additionally limited, e.g. by physical constraints in the operating room.

- **Low-dose CT denoising (LDCT-D):** Aims to remove noise from low-dose CT scans, enhancing image quality to a level comparable to standard-dose CT scans.
- **Compressed-sensing magnetic resonance imaging (CS-MRI):** Aims to reconstruct high-quality images from undersampled MRI data.
- **Z-axis super-resolution on MR images (ZSR-MRI):** Aims to enhance the resolution of MR images along the z-axis.
- **Standard-dose PET (SPET) scans from Low-dose PET (LPET) scans:** Aims to reconstruct high-quality PET images from low-dose PET scans.

While these tasks have extensively been explored on 2D images (sliced volumes), research on directly solving these problems on the 3D data is limited. An overview of publications on 3D medical image reconstruction is shown in Table 3.

Table 3 Overview of publications on 3D image reconstruction frameworks, the data modalities, public datasets used for training(– for private data), the solved tasks, as well as the utilized network architecture.

Study	Model	Modality	Dataset(s)	Task	Network(s)
Wolterink et al. (2017) [126]	GAN	CT	–	LDCT-D	3D GAN
Wang et al. (2018) [118]	GAN	PET	–	LPET-SPET	3D cGAN
Luo et al. (2021) [79]	GAN	PET	–	LPET-SPET	3D ViT-GAN
Zeng et al. (2022) [135]	GAN	PET	–	LPET-SPET	3D ViT-GAN
Xue et al. (2023) [130]	GAN	PET	Ultra-low Dose PET Imaging Challenge 2022	LPET-SPET	3D SRGAN
Wang et al. (2024) [117]	GAN	PET	–	LPET-SPET	3D ViT-GAN
Lee et al. (2023) [71]	DDM	CT, MRI	AAPM 2016 CT Low-Dose Grand Challenge	SV-CT, CS-MRI, ZSR-MRI	2D Score DDMs
Chung et al. (2023) [20]	DDM	CT, MRI	AAPM 2016 CT Low-Dose Grand Challenge, BRATS, fastMRI	SV-CT, LA-CT, CS-MRI	2D Score DDM
Xie et al. (2023) [129]	DDM	PET	–	LPET-SPET	2.5D DDPM/DDIM
He et al. (2024) [46]	DDM	CT, MRI	AAPM 2016 CT Low-Dose Grand Challenge, IXI	SV-CT, LA-CT, CS-MRI, ZSR-MRI	Triplane DDPM
Li et al. (2024) [75]	DDM	CT, MRI	AAPM 2016 CT Low-Dose Grand Challenge, BRATS	SV-CT, CS-MRI	2D Score DDMs

Several scientific challenges have drawn attention to the topic and provided valuable datasets for evaluating different image reconstruction approaches. These challenges include the AAPM 2016 CT Low-Dose Grand Challenge [82], the MICCAI 2021 Brain MRI Reconstruction Challenge with Realistic Noise [83], the MICCAI 2022 Ultra-low Dose PET Imaging Challenge [67], and the MICCAI 2023 Cardiac MRI Reconstruction Challenge [16]. Due to the computational complexity of directly handling 3D data, most presented approaches still operate on 2D slices, highlighting the need for efficient 3D backbones. Existing 3D GAN-based approaches have mostly focused on synthetic SPET image generation with conditional GAN [118], Vision

Transfomer GANs (ViT-GAN) [79, 117, 135] or Classification-Guided GAN [130] and operate on rather low-resolution volumes. Diffusion-based approaches primarily focused on SV-CT, LA-CT and CS-MRI. They formulate the task as an inverse problem of predicting an unknown image x given limited measurements y . The forward model is denoted as $y = \mathbf{A}x + \epsilon$, with \mathbf{A} being a degradation function (e.g. partial sampling of the sinogram for SV-CT and LA-CT, or k -space for CS-MRI) and the measuring noise ϵ . The inverse task $\hat{x} = G_\theta(y)$ is solved using a DGM G_θ . They address the problem of dealing with high-dimensional 3D data by applying perpendicular 2D models [71, 75], by conditioning the model on adjacent slices to form 2.5D models [129], or by applying 2D models to a triplane representation of the data [46].

Similar to image-to-image translation models, image reconstruction models can hallucinate structures that are not present in the actual anatomy, potentially leading to misdiagnosis. To ensure clinically relevant and reliable images, it is essential to develop robust models, compile comprehensive training datasets, and perform rigorous validation. In addition, these models should be used with caution and an understanding of the potential risks.

4 Evaluating Deep Generative Models

Evaluating deep generative models in medical imaging is not trivial and probably deserves its own chapter. Nevertheless, we will give a brief overview of popular metrics and discuss various image quality, diversity, utility, privacy, and other non-image-related metrics that should be considered when evaluating generative models and the data they synthesize.

4.1 Image Quality Metrics

The **Fréchet Inception Distance (FID)** [47] is a metric that measures image fidelity by comparing the distribution of real and generated images without requiring image pairs. It has widely been applied to evaluate unconditional image-generation tasks. The FID score is calculated by first extracting high-level features from real and synthetic images using an intermediate activation of a pre-trained neural network, calculating statistics over these features by fitting two multivariate Gaussians to the real $\mathcal{N}(\mu_r, \Sigma_r)$ and synthetic images features $\mathcal{N}(\mu_s, \Sigma_s)$, and computing the Fréchet distance between those distributions:

$$FID = \|\mu_r - \mu_s\|_2^2 + tr(\Sigma_r + \Sigma_s - 2\sqrt{\Sigma_r \Sigma_s}). \quad (7)$$

A small FID score indicates that the distributions of real and synthetic images are similar, suggesting that the model effectively learned the data distribution, which

results in a good visual appearance. In 3D medical image computing, Med3D-Net [15] has widely been applied as a feature extraction network. While FID scores are a useful tool for assessing image fidelity in unconditional image generation tasks, comparing these scores across publications is not straightforward and should be done cautiously. This is because FID scores are highly dependent on the choice of feature extraction network and the specific feature layer used. Further, metrics like FID, or variants like the Kernel Inception Distance (KID) [10], are highly dependent on a sufficiently large number of samples used to approximate the data distributions [19]. Without fulfilling this requirement, these metrics lose their meaningfulness, which is an often overlooked problem within limited data regimes such as medical imaging.

For image generation tasks where a ground truth image is available, such as a paired cross-modality image synthesis task, metrics like Peak Signal-to-Noise-Ratio (PSNR), Structural Similarity Index Measure (SSIM) or Mean Squared Error (MSE) can be applied to compare generated and ground truth image. The **Peak Signal-to-Noise-Ratio (PSNR)** is a metric originally used to measure the reconstruction quality of lossy compressed images. In the context of evaluating conditional image generation, it measures the fidelity of the synthetic image S compared to the real ground truth R and is defined as

$$PSNR = 10 \cdot \log_{10} \left(\frac{MAX_R^2}{MSE} \right) = 20 \cdot \log_{10}(MAX_R) - 10 \cdot \log_{10}(MSE), \quad (8)$$

with MAX_R being the maximum possible intensity value of the images, usually 255 for uint8 grayscale images, and the **Mean Squared Error (MSE)** between real and synthetic image, which is defined over all voxels N of the volume:

$$MSE = \frac{1}{N} \sum_{i=1}^N (R_i - S_i)^2. \quad (9)$$

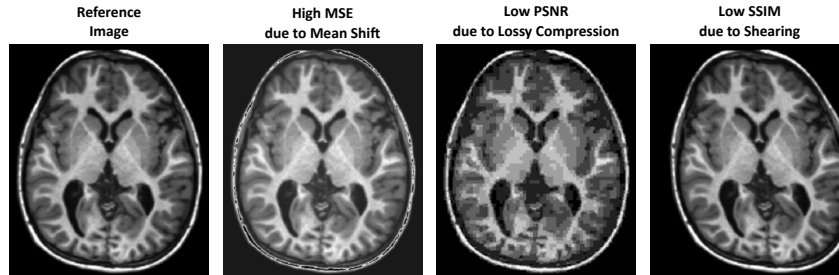


Fig. 7 Paired Image Quality Metrics. Paired Metrics allow quantifying the similarity of synthetic or corrupted images to a reference image (first column). Examples include the *Mean Squared Error (MSE)*, commonly used to quantify noise artifacts (second column), the *Peak Signal-to-Noise-Ratio (PSNR)*, often used to quantify compression quality (third column), as well as the *Structural Similarity Index Measure (SSIM)* to evaluate structural distortions (fourth column).

While PSNR and MSE are widely applied metrics for assessing image quality, they have several limitations. As pixel-level metrics, they can't capture any structural information that is strongly correlated with good visual perception of the generated images. [119] This drawback led to the development of the **Structural Similarity Index Measure (SSIM)**, which evaluates the perceived change in structural information, luminance, and contrast. It is computed over a shifting window of similar size, e.g. $11 \times 11 \times 11$, denoted as r for a window of R and s for the same window from S . The SSIM is defined as:

$$SSIM = \frac{(2\mu_r\mu_s + c_1)(2\sigma_{rs} + c_2)}{(\mu_r^2 + \mu_s^2 + c_1)(\sigma_r^2 + \sigma_s^2 + c_2)} \quad (10)$$

with the mean μ_r and μ_s , and variances σ_r^2 and σ_s^2 over the respective windows pixel intensities, the covariance σ_{rs} between them, as well as two constants c_1 and c_2 to numerically stabilize the score against division with weak denominators. While a small SSIM score indicates that two images significantly differ in structural information, luminance and contrast, a score close to 1 indicates high image similarity. Example image variations corresponding to significant changes in MSE, PSNR and SSIM scores are visualized in Figure 7. In addition to the classic SSIM score, several variants such as MS-SSIM [120], or 4-(G-)SSIM [73] have been proposed to improve the quality metric further. A competitive evaluation of several SSIM versions on radiology images has been performed in [96], suggesting that 4-MS-G-SSIM provides optimal results and strongly agrees with human perception. Other ways to assess image quality are the **Inception Score** [102], **Precision** [69, 101], or by conduction a **Visual Turing Test** [37].

4.2 Image Diversity Metrics

While the **Structural Similarity Index Measure (SSIM)** can be used to measure the similarity between image pairs, it has also been applied to assess the diversity of the generated images in unconditional generation tasks, an important factor to consider when evaluating the performance of generative models. In [33] and [93], the authors measure image diversity by averaging the MS-SSIM over generated images by iteratively comparing a reference image to all other generated images. A low SSIM in this case indicates high generation diversity, meaning that the generated images are not similar to each other. Such quantification of diversity can also be carried out in the feature space of pre-trained feature extractors, using similarity metrics like LPIPS [137].

Another common way to assess image diversity is the **Recall Score** [69, 101], which measures the fraction of the training data manifold that can be produced by the generative network. Similar to computing the FID score, a feature extraction network is applied to produce a set of high-level features of real Φ_r and synthetic images Φ_s . A feature vector of a single image is denoted as ϕ_r for a real image and

as ϕ_s for a synthetic image. The Recall score is then defined as

$$\text{Recall} = \frac{1}{|\Phi_r|} \sum_{\phi_r \in \Phi_r} f(\phi_r, \Phi_s) \quad (11)$$

with $|\Phi_r|$ being the number of images to compute the score, and $f(\phi_r, \Phi_s)$ a nearest-neighbor-based binary function that determines whether a real image could be generated by evaluating whether it lays within the approximated synthetic data distribution. A high recall score indicates that the trained network generates diverse samples from the entire data distribution, while a low recall score could be a sign of mode collapse.

4.3 Utility & Privacy Metrics

Another common way to evaluate the performance of deep generative networks is to assess the utility of the generated data by measuring **performance improvements on relevant downstream tasks** when trained with additional synthetic data. In medical image computing, this has, for example, been done by measuring performance improvements of classification [32, 35, 100] or segmentation [1] tasks.

Since deep generative models are known to memorize data [12, 21, 42], assessing the privacy of synthetic images and minimizing the risk of re-identification [30, 132] before sharing images or weights of models trained on non-public data is crucial. To evaluate the privacy of generated images, metrics such as the **Rarity Score** [44] or **Average Minimum Cosine Distance (AMD)** [3], which measures the uncommonness of generated images as the nearest-neighbor distance of real and synthetic data points in a latent space, have been proposed. Other privacy metrics rely on **model-based re-identification** [88] or apply **Extraction Attacks** [13] to measure privacy by trying to extract training images from the trained models.

4.4 Non-Image Metrics

In addition to the previously discussed image metrics, other factors such as the model’s **Inference Time**, **Computational Efficiency**, usually measured in Floating Point Operations (FLOPs), or **Memory Consumption** must also be considered in the evaluation to ensure the model’s applicability to real-world problems. This is especially important for time-critical applications or when the method is to be used in a resource-constrained environment. The **Ethical and Social Impact** of the model, i.e. possible bias and fairness of the model as well as potential misuse, should also be considered.

5 Current Challenges & Conclusion

Despite the recent success of deep generative models in medical imaging, many essential and critical challenges remain. This section overviews such open challenges and potential directions for future research.

5.1 Challenges

High-resolution data is crucial for a thorough and accurate analysis of medical images. However, many current deep generative models struggle with scaling to such high-dimensional spaces. Additionally, computational resources are often limited in clinical settings, making in-house training of large-scale generative models nearly impossible. Furthermore, medical image analysis often benefits from longitudinal data, e.g. repeated scans of patients at progressive points in time. Modeling such temporal data with generative models further increases the required compute significantly and is an open and highly relevant research direction [95, 109, 133, 141]. To address these challenges, various methods have been proposed to significantly reduce the number of model parameters, speed up training and inference times, and lower GPU memory requirements. Notable approaches include WDMs [33, 92] and Neural Cellular Automata [56]. Despite these advancements, the **need for scalable and efficient models** continues to drive further research in this area.

The scalability problem also applies to the data itself. Many state-of-the-art generative models are trained on excessive amounts of data that are typically unavailable for most medical problems. Collecting and annotating such data can be a resource- and labor-intensive process, further complicated by regulatory issues. In addition, the datasets used to train generative models should be as diverse and representative as possible to avoid the negative effects of bias. One way to mitigate these problems and allow for the development of a robust and useful model is to **provide data in an open access paradigm**. Another way to effectively train generative models and fully capture complex data distributions is to **develop efficient methods for federated learning** [38, 54, 111] and solve existing problems related to this. An example of such issues could be the case where a patient - or even an entire institute - opts out of a study and withdraws its samples from the training distribution. The process of unlearning [36], therefore, needs to be addressed in the context of generative models for medical imaging.

Another commonly faced challenge is related to the evaluation of DGMs in the medical domain. Most metrics widely used to evaluate generative models in the natural image domain must only be carefully applied to medical images. These metrics might only provide reliable quantitative results with adequately pre-trained feature extractors [7] and an appropriately large test sample size [19]. In addition, the three-dimensionality of medical imaging data is often not considered in such metrics, e.g. feature extractors for 3D data might not be publicly available and have to be

built from scratch. We, therefore, identify the **need for more rigorous quantitative testing of generative models in the medical domain**.

Further challenges arise when it comes to safely deploying these algorithms, as generative models can pose the threat of (unconscious or deliberate) data corruption [45]. Especially when these models are deployed as a data augmentation method for downstream task models, additional curation is needed to minimize the risk of error propagation from the generative to the downstream task model [113]. Additionally, the risk of these models hallucinating can potentially lead to drastic consequences, e.g. for the tasks of reconstruction or inpainting in the medical domain.

Most generative models in the medical domain are developed and trained on publicly available data. In some cases, in which private data cohorts are also considered, privacy protection is an important issue that needs to be taken into account. Even releasing the weights of generative models trained on private data could lead to privacy violations, since the training data can essentially be extracted from these models [13]. The problem of **privacy preserving generative models** needs to be addressed and is an interesting and promising direction for future research.

5.2 Conclusion

Deep generative models have achieved significant success in recent years, proving to be a valuable tool for learning complex data distributions and solving medically relevant downstream tasks. We reviewed the background of Variational Autoencoders, Generative Adversarial Networks, and Denoising Diffusion Models, highlighting their strengths and weaknesses. In addition, we demonstrated their application to tasks such as unconditional image generation, image-to-image translation, and image reconstruction, and discussed commonly used evaluation metrics as well as pitfalls associated with these metrics.

Despite the mentioned advances in DGMs for 3D medical image synthesis, several open challenges remain that motivate future research in this area. Finding novel, more efficient data representations, developing tools for federated learning, or exploring methods to address unlearning and privacy concerns are critical to advancing the capabilities of deep generative models in the medical domain. The goal of these efforts is to create efficient, fair, and reliable algorithms that can provide physicians with valuable insights and ultimately improve personalized medicine, enhance predictive analytics, and facilitate the development of new therapeutic strategies.

Acknowledgements This work was financially supported by the Werner Siemens Foundation through the MIRACLE II project.

Competing Interests The authors have no conflicts of interest to declare that are relevant to the content of this chapter.

References

1. Al Khalil, Y., Amirrajab, S., Lorenz, C., Weese, J., Pluim, J., Breeuwer, M.: On the usability of synthetic data for improving the robustness of deep learning-based segmentation of cardiac magnetic resonance images. *Medical Image Analysis* **84**, 102688 (2023)
2. Arjovsky, M., Chintala, S., Bottou, L.: Wasserstein generative adversarial networks. In: *International conference on machine learning*, pp. 214–223. PMLR (2017)
3. Bai, C.Y., Lin, H.T., Raffel, C., Kan, W.C.w.: On training sample memorization: Lessons from benchmarking generative modeling with a large-scale competition. In: *Proceedings of the 27th ACM SIGKDD conference on knowledge discovery & data mining*, pp. 2534–2542 (2021)
4. Bakas, S., Akbari, H., Sotiras, A., Bilello, M., Rozycki, M., Kirby, J.S., Freymann, J.B., Farahani, K., Davatzikos, C.: Advancing the cancer genome atlas glioma mri collections with expert segmentation labels and radiomic features. *Scientific data* **4**(1), 1–13 (2017)
5. Bakas, S., Reyes, M., Jakab, A., Bauer, S., Rempfler, M., Crimi, A., Shinohara, R.T., Berger, C., Ha, S.M., Rozycki, M., et al.: Identifying the best machine learning algorithms for brain tumor segmentation, progression assessment, and overall survival prediction in the brats challenge. *arXiv preprint arXiv:1811.02629* (2018)
6. Baltruschat, I.M., Janbakhshi, P., Lenga, M.: Brasyn 2023 challenge: Missing mri synthesis and the effect of different learning objectives. *arXiv preprint arXiv:2403.07800* (2024)
7. Barratt, S., Sharma, R.: A note on the inception score. *arXiv preprint arXiv:1801.01973* (2018)
8. Bazangani, F., Richard, F.J., Ghattas, B., Guedj, E.: Fdg-pet to t1 weighted mri translation with 3d elicit generative adversarial network (e-gan). *Sensors* **22**(12), 4640 (2022)
9. Bergen, R.V., Rajotte, J.F., Yousefirizi, F., Klyuzhin, I.S., Rahmim, A., Ng, R.T.: 3d pet image generation with tumour masks using tgan. In: *Medical Imaging 2022: Image Processing*, vol. 12032, pp. 459–469. SPIE (2022)
10. Bińkowski, M., Sutherland, D.J., Arbel, M., Gretton, A.: Demystifying mmd gans. In: *International Conference on Learning Representations* (2018)
11. Brock, A., Donahue, J., Simonyan, K.: Large scale gan training for high fidelity natural image synthesis. In: *International Conference on Learning Representations* (2018)
12. van den Burg, G., Williams, C.: On memorization in probabilistic deep generative models. *Advances in Neural Information Processing Systems* **34**, 27916–27928 (2021)
13. Carlini, N., Hayes, J., Nasr, M., Jagielski, M., Sehwag, V., Tramèr, F., Balle, B., Ippolito, D., Wallace, E.: Extracting training data from diffusion models. In: *32nd USENIX Security Symposium (USENIX Security 23)*, pp. 5253–5270 (2023)
14. Carreira, J., Zisserman, A.: Quo vadis, action recognition? a new model and the kinetics dataset. In: *proceedings of the IEEE Conference on Computer Vision and Pattern Recognition*, pp. 6299–6308 (2017)
15. Chen, S., Ma, K., Zheng, Y.: Med3d: Transfer learning for 3d medical image analysis. *arXiv preprint arXiv:1904.00625* (2019)
16. Chengyan, W., Xinyu, Z., Xutong, K., Chen, Q., Shuo, W., Jun, L., Jing, Q., Yapeng, T., He, W., Zhensen, C., Xiahai, Z., Sha, H., Ying-Hua, C., Weibo, C.: Cardiac mri reconstruction challenge (2023). DOI 10.5281/zenodo.7840229
17. Chilamkurthy, S., Ghosh, R., Tanamala, S., Biviji, M., Campeau, N.G., Venugopal, V.K., Mahajan, V., Rao, P., Warier, P.: Development and validation of deep learning algorithms for detection of critical findings in head ct scans. *arXiv preprint arXiv:1803.05854* (2018)
18. Chong, C.K., Ho, E.T.W.: Synthesis of 3d mri brain images with shape and texture generative adversarial deep neural networks. *IEEE Access* **9**, 64747–64760 (2021)
19. Chong, M.J., Forsyth, D.: Effectively unbiased fid and inception score and where to find them. In: *Proceedings of the IEEE/CVF conference on computer vision and pattern recognition*, pp. 6070–6079 (2020)
20. Chung, H., Ryu, D., McCann, M.T., Klasky, M.L., Ye, J.C.: Solving 3d inverse problems using pre-trained 2d diffusion models. In: *Proceedings of the IEEE/CVF Conference on Computer Vision and Pattern Recognition*, pp. 22542–22551 (2023)

21. Dar, S.U.H., Seyfarth, M., Kahmann, J., Ayx, I., Papavassiliu, T., Schoenberg, S.O., Engelhardt, S.: Unconditional latent diffusion models memorize patient imaging data. arXiv preprint arXiv:2402.01054 (2024)
22. Deng, J., Dong, W., Socher, R., Li, L.J., Li, K., Fei-Fei, L.: Imagenet: A large-scale hierarchical image database. In: 2009 IEEE conference on computer vision and pattern recognition, pp. 248–255. Ieee (2009)
23. Dhariwal, P., Nichol, A.: Diffusion models beat gans on image synthesis. *Advances in neural information processing systems* **34**, 8780–8794 (2021)
24. Dorjsembe, Z., Odonchimed, S., Xiao, F.: Three-dimensional medical image synthesis with denoising diffusion probabilistic models. In: *Medical Imaging with Deep Learning* (2022)
25. Dorjsembe, Z., Pao, H.K., Odonchimed, S., Xiao, F.: Conditional diffusion models for semantic 3d brain mri synthesis. *IEEE Journal of Biomedical and Health Informatics* (2024)
26. Durrer, A., Wolleb, J., Bieder, F., Friedrich, P., Melie-Garcia, L., Ocampo-Pineda, M., Bercea, C.I., Hamamci, I.E., Wiestler, B., Piraud, M., et al.: Denoising diffusion models for 3d healthy brain tissue inpainting. arXiv preprint arXiv:2403.14499 (2024)
27. Durrer, A., Wolleb, J., Bieder, F., Sinnecker, T., Weigel, M., Sandkuehler, R., Granziera, C., Yaldizli, Ö., Cattin, P.C.: Diffusion models for contrast harmonization of magnetic resonance images. In: *Medical Imaging with Deep Learning* (2023)
28. Esser, P., Rombach, R., Ommer, B.: Taming transformers for high-resolution image synthesis. In: *Proceedings of the IEEE/CVF conference on computer vision and pattern recognition*, pp. 12873–12883 (2021)
29. Fernandez, V., Pinaya, W.H.L., Borges, P., Graham, M.S., Vercauteren, T., Cardoso, M.J.: A 3d generative model of pathological multi-modal mr images and segmentations. In: *International Conference on Medical Image Computing and Computer-Assisted Intervention*, pp. 132–142. Springer (2023)
30. Fernandez, V., Sanchez, P., Pinaya, W.H.L., Jacenków, G., Tsiftaris, S.A., Cardoso, M.J.: Privacy distillation: Reducing re-identification risk of diffusion models. In: *International Conference on Medical Image Computing and Computer-Assisted Intervention*, pp. 3–13. Springer (2023)
31. Freund, Y., Haussler, D.: Unsupervised learning of distributions on binary vectors using two layer networks. *Advances in neural information processing systems* **4** (1991)
32. Frid-Adar, M., Diamant, I., Klang, E., Amitai, M., Goldberger, J., Greenspan, H.: Gan-based synthetic medical image augmentation for increased cnn performance in liver lesion classification. *Neurocomputing* **321**, 321–331 (2018)
33. Friedrich, P., Wolleb, J., Bieder, F., Durrer, A., Cattin, P.C.: Wdm: 3d wavelet diffusion models for high-resolution medical image synthesis. arXiv preprint arXiv:2402.19043 (2024)
34. Friedrich, P., Wolleb, J., Bieder, F., Thieringer, F.M., Cattin, P.C.: Point cloud diffusion models for automatic implant generation. In: *International Conference on Medical Image Computing and Computer-Assisted Intervention*, pp. 112–122. Springer (2023)
35. Frisch, Y., Fuchs, M., Sanner, A., Ucar, F.A., Frenzel, M., Wasielica-Poslednik, J., Gericke, A., Wagner, F.M., Dratsch, T., Mukhopadhyay, A.: Synthesising rare cataract surgery samples with guided diffusion models. In: *International Conference on Medical Image Computing and Computer-Assisted Intervention*, pp. 354–364. Springer (2023)
36. Gandikota, R., Materzynska, J., Fiotto-Kaufman, J., Bau, D.: Erasing concepts from diffusion models. In: *Proceedings of the IEEE/CVF International Conference on Computer Vision*, pp. 2426–2436 (2023)
37. Geman, D., Geman, S., Hallonquist, N., Younes, L.: Visual turing test for computer vision systems. *Proceedings of the National Academy of Sciences* **112**(12), 3618–3623 (2015)
38. de Goede, M., Cox, B., Decouchant, J.: Training diffusion models with federated learning. arXiv preprint arXiv:2406.12575 (2024)
39. Goodfellow, I., Pouget-Abadie, J., Mirza, M., Xu, B., Warde-Farley, D., Ozair, S., Courville, A., Bengio, Y.: Generative adversarial nets. *Advances in neural information processing systems* **27** (2014)

40. Graf, R., Schmitt, J., Schlaeger, S., Möller, H.K., Sideri-Lampretsa, V., Sekuboyina, A., Krieg, S.M., Wiestler, B., Menze, B., Rueckert, D., et al.: Denoising diffusion-based mri to ct image translation enables automated spinal segmentation. *European Radiology Experimental* **7**(1), 70 (2023)
41. Granstedt, J.L., Kelkar, V.A., Zhou, W., Anastasio, M.A.: Slabgan: a method for generating efficient 3d anisotropic medical volumes using generative adversarial networks. In: *Medical Imaging 2021: Image Processing*, vol. 11596, pp. 329–335. SPIE (2021)
42. Gu, X., Du, C., Pang, T., Li, C., Lin, M., Wang, Y.: On memorization in diffusion models. *arXiv preprint arXiv:2310.02664* (2023)
43. Gulrajani, I., Ahmed, F., Arjovsky, M., Dumoulin, V., Courville, A.C.: Improved training of wasserstein gans. *Advances in neural information processing systems* **30** (2017)
44. Han, J., Choi, H., Choi, Y., Kim, J., Ha, J.W., Choi, J.: Rarity score: A new metric to evaluate the uncommonness of synthesized images. In: *The Eleventh International Conference on Learning Representations* (2022)
45. Hataya, R., Bao, H., Arai, H.: Will large-scale generative models corrupt future datasets? In: *2023 IEEE/CVF International Conference on Computer Vision (ICCV)*, pp. 20498–20508. IEEE (2023)
46. He, J., Li, B., Yang, G., Liu, Z.: Blaze3dm: Marry triplane representation with diffusion for 3d medical inverse problem solving. *arXiv preprint arXiv:2405.15241* (2024)
47. Heusel, M., Ramsauer, H., Unterthiner, T., Nessler, B., Hochreiter, S.: Gans trained by a two time-scale update rule converge to a local nash equilibrium. *Advances in neural information processing systems* **30** (2017)
48. Ho, J., Jain, A., Abbeel, P.: Denoising diffusion probabilistic models. *Advances in neural information processing systems* **33**, 6840–6851 (2020)
49. Hong, S., Marinescu, R., Dalca, A.V., Bonkhoff, A.K., Bretzner, M., Rost, N.S., Golland, P.: 3d-stylegan: A style-based generative adversarial network for generative modeling of three-dimensional medical images. In: *Deep Generative Models, and Data Augmentation, Labelling, and Imperfections: First Workshop, DGM4MICCAI 2021, and First Workshop, DALI 2021, Held in Conjunction with MICCAI 2021, Strasbourg, France, October 1, 2021, Proceedings 1*, pp. 24–34. Springer (2021)
50. Hu, Q., Li, H., Zhang, J.: Domain-adaptive 3d medical image synthesis: An efficient unsupervised approach. In: *International Conference on Medical Image Computing and Computer-Assisted Intervention*, pp. 495–504. Springer (2022)
51. Hu, S., Lei, B., Wang, S., Wang, Y., Feng, Z., Shen, Y.: Bidirectional mapping generative adversarial networks for brain mr to pet synthesis. *IEEE Transactions on Medical Imaging* **41**(1), 145–157 (2021)
52. Huijben, E., Terpstra, M.L., Galapon Jr, A., Pai, S., Thummerer, A., Koopmans, P., Afonso, M., van Eijnatten, M., Gurney-Champion, O., Chen, Z., et al.: Generating synthetic computed tomography for radiotherapy: Synthrad2023 challenge report. *arXiv preprint arXiv:2403.08447* (2024)
53. III, A., et al.: The lung image database consortium (lidc) and image database resource initiative (idri): a completed reference database of lung nodules on ct scans. *Medical physics* **38**(2), 915–931 (2011)
54. Jothiraj, F.V.S., Mashhadi, A.: Phoenix: A federated generative diffusion model. *arXiv preprint arXiv:2306.04098* (2023)
55. Kalantar, R., Hindocha, S., Hunter, B., Sharma, B., Khan, N., Koh, D.M., Ahmed, M., Aboagye, E.O., Lee, R.W., Blackledge, M.D.: Non-contrast ct synthesis using patch-based cycle-consistent generative adversarial network (cycle-gan) for radiomics and deep learning in the era of covid-19. *Scientific Reports* **13**(1), 10568 (2023)
56. Kalkhof, J., Kühn, A., Frisch, Y., Mukhopadhyay, A.: Frequency-time diffusion with neural cellular automata. *arXiv preprint arXiv:2401.06291* (2024)
57. Kapoor, J., Macke, J.H., Baumgartner, C.F.: Multiscale metamorphic vae for 3d brain mri synthesis. *arXiv preprint arXiv:2301.03588* (2023)

58. Karras, T., Laine, S., Aittala, M., Hellsten, J., Lehtinen, J., Aila, T.: Analyzing and improving the image quality of stylegan. In: Proceedings of the IEEE/CVF conference on computer vision and pattern recognition, pp. 8110–8119 (2020)
59. Khader, F., Müller-Franzes, G., Tayebi Arasteh, S., Han, T., Haarbuerger, C., Schulze-Hagen, M., Schad, P., Engelhardt, S., Baeßler, B., Foersch, S., et al.: Denoising diffusion probabilistic models for 3d medical image generation. *Scientific Reports* **13**(1), 7303 (2023)
60. Khosla, A., Jayadevaprakash, N., Yao, B., Fei-Fei, L.: Novel dataset for fine-grained image categorization. In: First Workshop on Fine-Grained Visual Categorization, IEEE Conference on Computer Vision and Pattern Recognition (2011)
61. Kim, B., Han, I., Ye, J.C.: Diffusemorph: Unsupervised deformable image registration using diffusion model. In: European conference on computer vision, pp. 347–364. Springer (2022)
62. Kim, J., Li, Y., Shin, B.S.: 3d-dggan: A data-guided generative adversarial network for high fidelity in medical image generation. *IEEE Journal of Biomedical and Health Informatics* (2024)
63. Kim, J., Park, H.: Adaptive latent diffusion model for 3d medical image to image translation: Multi-modal magnetic resonance imaging study. In: Proceedings of the IEEE/CVF Winter Conference on Applications of Computer Vision, pp. 7604–7613 (2024)
64. Kingma, D.P., Welling, M.: Auto-encoding variational bayes. arXiv preprint arXiv:1312.6114 (2013)
65. Konz, N., Chen, Y., Dong, H., Mazurowski, M.A.: Anatomically-controllable medical image generation with segmentation-guided diffusion models. arXiv preprint arXiv:2402.05210 (2024)
66. Ktena, I., Wiles, O., Albuquerque, I., Rebuffi, S.A., Tanno, R., Roy, A.G., Azizi, S., Belgrave, D., Kohli, P., Cemgil, T., et al.: Generative models improve fairness of medical classifiers under distribution shifts. *Nature Medicine* pp. 1–8 (2024)
67. Kuangyu, S., Rui, G., Song, X., Axel, R., Biao, L.: Ultra-low dose pet imaging challenge 2022 (2022). URL <https://doi.org/10.5281/zenodo.6361846>
68. Kwon, G., Han, C., Kim, D.s.: Generation of 3d brain mri using auto-encoding generative adversarial networks. In: International Conference on Medical Image Computing and Computer-Assisted Intervention, pp. 118–126. Springer (2019)
69. Kynkäänniemi, T., Karras, T., Laine, S., Lehtinen, J., Aila, T.: Improved precision and recall metric for assessing generative models. *Advances in neural information processing systems* **32** (2019)
70. Lan, H., Initiative, A.D.N., Toga, A.W., Sepehrband, F.: Three-dimensional self-attention conditional gan with spectral normalization for multimodal neuroimaging synthesis. *Magnetic resonance in medicine* **86**(3), 1718–1733 (2021)
71. Lee, S., Chung, H., Park, M., Park, J., Ryu, W.S., Ye, J.C.: Improving 3d imaging with pre-trained perpendicular 2d diffusion models. In: Proceedings of the IEEE/CVF International Conference on Computer Vision, pp. 10710–10720 (2023)
72. Li, A.C., Prabhudesai, M., Duggal, S., Brown, E., Pathak, D.: Your diffusion model is secretly a zero-shot classifier. In: Proceedings of the IEEE/CVF International Conference on Computer Vision, pp. 2206–2217 (2023)
73. Li, C., Bovik, A.C.: Content-partitioned structural similarity index for image quality assessment. *Signal Processing: Image Communication* **25**(7), 517–526 (2010)
74. Li, Y., Yakushev, I., Hedderich, D.M., Wachinger, C.: Pasta: Pathology-aware mri to pet cross-modal translation with diffusion models. arXiv preprint arXiv:2405.16942 (2024)
75. Li, Z., Wang, Y., Zhang, J., Wu, W., Yu, H.: Two-and-a-half order score-based model for solving 3d ill-posed inverse problems. *Computers in Biology and Medicine* **168**, 107819 (2024)
76. Lin, W., Lin, W., Chen, G., Zhang, H., Gao, Q., Huang, Y., Tong, T., Du, M., Initiative, A.D.N.: Bidirectional mapping of brain mri and pet with 3d reversible gan for the diagnosis of alzheimer’s disease. *Frontiers in Neuroscience* **15**, 646013 (2021)
77. Liu, Y., Dwivedi, G., Boussaid, F., Sanfilippo, F., Yamada, M., Bennamoun, M.: Inflating 2d convolution weights for efficient generation of 3d medical images. *Computer Methods and Programs in Biomedicine* **240**, 107685 (2023)

78. Luo, S., Hu, W.: Diffusion probabilistic models for 3d point cloud generation. In: Proceedings of the IEEE/CVF Conference on Computer Vision and Pattern Recognition, pp. 2837–2845 (2021)
79. Luo, Y., Wang, Y., Zu, C., Zhan, B., Wu, X., Zhou, J., Shen, D., Zhou, L.: 3d transformer-gan for high-quality pet reconstruction. In: Medical Image Computing and Computer Assisted Intervention–MICCAI 2021: 24th International Conference, Strasbourg, France, September 27–October 1, 2021, Proceedings, Part VI 24, pp. 276–285. Springer (2021)
80. Lutz, S., Amliantitis, K., Smolic, A.: Alphagan: Generative adversarial networks for natural image matting. arXiv preprint arXiv:1807.10088 (2018)
81. Mao, X., Li, Q., Xie, H., Lau, R.Y., Wang, Z., Paul Smolley, S.: Least squares generative adversarial networks. In: Proceedings of the IEEE international conference on computer vision, pp. 2794–2802 (2017)
82. McCollough, C.H., Bartley, A.C., Carter, R.E., Chen, B., Drees, T.A., Edwards, P., Holmes III, D.R., Huang, A.E., Khan, F., Leng, S., et al.: Low-dose ct for the detection and classification of metastatic liver lesions: results of the 2016 low dose ct grand challenge. *Medical physics* **44**(10), e339–e352 (2017)
83. Melanie, G., Hannah, E.: Brain mri reconstruction challenge with realistic noise (2021). URL <https://doi.org/10.5281/zenodo.4572640>
84. Mensing, D., Hirsch, J., Wenzel, M., Günther, M.: 3d (c) gan for whole body mr synthesis. In: MICCAI Workshop on Deep Generative Models, pp. 97–105. Springer (2022)
85. Menze, B.H., Jakab, A., Bauer, S., Kalpathy-Cramer, J., Farahani, K., Kirby, J., Burren, Y., Porz, N., Slotboom, J., Wiest, R., et al.: The multimodal brain tumor image segmentation benchmark (brats). *IEEE transactions on medical imaging* **34**(10), 1993–2024 (2014)
86. Miyato, T., Kataoka, T., Koyama, M., Yoshida, Y.: Spectral normalization for generative adversarial networks. In: International Conference on Learning Representations (2018)
87. Oord, A.v.d., Dieleman, S., Zen, H., Simonyan, K., Vinyals, O., Graves, A., Kalchbrenner, N., Senior, A., Kavukcuoglu, K.: Wavenet: A generative model for raw audio. arXiv preprint arXiv:1609.03499 (2016)
88. Packhäuser, K., Gündel, S., Münster, N., Syben, C., Christlein, V., Maier, A.: Deep learning-based patient re-identification is able to exploit the biometric nature of medical chest x-ray data. *Scientific Reports* **12**(1), 14851 (2022)
89. Pan, S., Abouei, E., Wynne, J., Chang, C.W., Wang, T., Qiu, R.L., Li, Y., Peng, J., Roper, J., Patel, P., et al.: Synthetic ct generation from mri using 3d transformer-based denoising diffusion model. *Medical Physics* **51**(4), 2538–2548 (2024)
90. Pan, S., Chang, C.W., Peng, J., Zhang, J., Qiu, R.L., Wang, T., Roper, J., Liu, T., Mao, H., Yang, X.: Cycle-guided denoising diffusion probability model for 3d cross-modality mri synthesis. arXiv preprint arXiv:2305.00042 (2023)
91. Peng, W., Adeli, E., Bosschieter, T., Park, S.H., Zhao, Q., Pohl, K.M.: Generating realistic brain mris via a conditional diffusion probabilistic model. In: International Conference on Medical Image Computing and Computer-Assisted Intervention, pp. 14–24. Springer (2023)
92. Phung, H., Dao, Q., Tran, A.: Wavelet diffusion models are fast and scalable image generators. In: Proceedings of the IEEE/CVF Conference on Computer Vision and Pattern Recognition, pp. 10199–10208 (2023)
93. Pinaya, W.H., Tudosi, P.D., Dafflon, J., Da Costa, P.F., Fernandez, V., Nachev, P., Ourselin, S., Cardoso, M.J.: Brain imaging generation with latent diffusion models. In: MICCAI Workshop on Deep Generative Models, pp. 117–126. Springer (2022)
94. Poonkodi, S., Kanchana, M.: 3d-medtrancsgan: 3d medical image transformation using csgan. *Computers in Biology and Medicine* **153**, 106541 (2023)
95. Puglisi, L., Alexander, D.C., Ravi, D.: Enhancing spatiotemporal disease progression models via latent diffusion and prior knowledge. arXiv preprint arXiv:2405.03328 (2024)
96. Renieblas, G.P., Nogués, A.T., González, A.M., Gómez-Leon, N., Del Castillo, E.G.: Structural similarity index family for image quality assessment in radiological images. *Journal of medical imaging* **4**(3), 035501–035501 (2017)
97. Rezende, D., Mohamed, S.: Variational inference with normalizing flows. In: International conference on machine learning, pp. 1530–1538. PMLR (2015)

98. Rezende, D.J., Mohamed, S., Wierstra, D.: Stochastic backpropagation and approximate inference in deep generative models. In: International conference on machine learning, pp. 1278–1286. PMLR (2014)
99. Rombach, R., Blattmann, A., Lorenz, D., Esser, P., Ommer, B.: High-resolution image synthesis with latent diffusion models. In: Proceedings of the IEEE/CVF conference on computer vision and pattern recognition, pp. 10684–10695 (2022)
100. Sagers, L.W., Diao, J.A., Melas-Kyriazi, L., Groh, M., Rajpurkar, P., Adamson, A.S., Rotemberg, V., Daneshjou, R., Manrai, A.K.: Augmenting medical image classifiers with synthetic data from latent diffusion models. arXiv preprint arXiv:2308.12453 (2023)
101. Sajjadi, M.S., Bachem, O., Lucic, M., Bousquet, O., Gelly, S.: Assessing generative models via precision and recall. *Advances in neural information processing systems* **31** (2018)
102. Salimans, T., Goodfellow, I., Zaremba, W., Cheung, V., Radford, A., Chen, X.: Improved techniques for training gans. *Advances in neural information processing systems* **29** (2016)
103. Sanchez, P., Kascenas, A., Liu, X., O’Neil, A.Q., Tsafaris, S.A.: What is healthy? generative counterfactual diffusion for lesion localization. In: MICCAI Workshop on Deep Generative Models, pp. 34–44. Springer (2022)
104. Segato, A., Corbetta, V., Di Marzo, M., Pozzi, L., De Momi, E.: Data augmentation of 3d brain environment using deep convolutional refined auto-encoding alpha gan. *IEEE Transactions on Medical Robotics and Bionics* **3**(1), 269–272 (2020)
105. Sikka, A., Virk, J.S., Bathula, D.R., et al.: Mri to pet cross-modality translation using globally and locally aware gan (gla-gan) for multi-modal diagnosis of alzheimer’s disease. arXiv preprint arXiv:2108.02160 (2021)
106. Sohl-Dickstein, J., Weiss, E., Maheswaranathan, N., Ganguli, S.: Deep unsupervised learning using nonequilibrium thermodynamics. In: International conference on machine learning, pp. 2256–2265. PMLR (2015)
107. Song, J., Meng, C., Ermon, S.: Denoising diffusion implicit models. arXiv preprint arXiv:2010.02502 (2020)
108. Song, Y., Dhariwal, P., Chen, M., Sutskever, I.: Consistency models. In: Proceedings of the 40th International Conference on Machine Learning, pp. 32211–32252 (2023)
109. Stolt-Ans6, N., McGinnis, J., Pan, J., Hammernik, K., Rueckert, D.: Nisf: Neural implicit segmentation functions. In: International Conference on Medical Image Computing and Computer-Assisted Intervention, pp. 734–744. Springer (2023)
110. Sun, L., Chen, J., Xu, Y., Gong, M., Yu, K., Batmanghelich, K.: Hierarchical amortized gan for 3d high resolution medical image synthesis. *IEEE journal of biomedical and health informatics* **26**(8), 3966–3975 (2022)
111. Tun, Y.L., Thwal, C.M., Yoon, J.S., Kang, S.M., Zhang, C., Hong, C.S.: Federated learning with diffusion models for privacy-sensitive vision tasks. In: 2023 International Conference on Advanced Technologies for Communications (ATC), pp. 305–310. IEEE (2023)
112. Uzunova, H., Ehrhardt, J., Handels, H.: Memory-efficient gan-based domain translation of high resolution 3d medical images. *Computerized Medical Imaging and Graphics* **86**, 101801 (2020)
113. Van Breugel, B., Qian, Z., Van Der Schaar, M.: Synthetic data, real errors: how (not) to publish and use synthetic data. In: International Conference on Machine Learning, pp. 34793–34808. PMLR (2023)
114. Van Den Oord, A., Vinyals, O., et al.: Neural discrete representation learning. *Advances in neural information processing systems* **30** (2017)
115. Vaswani, A., Shazeer, N., Parmar, N., Uszkoreit, J., Jones, L., Gomez, A.N., Kaiser, L., Polosukhin, I.: Attention is all you need. *Advances in neural information processing systems* **30** (2017)
116. Volokitin, A., Erdil, E., Karani, N., Tezcan, K.C., Chen, X., Van Gool, L., Konukoglu, E.: Modelling the distribution of 3d brain mri using a 2d slice vae. In: Medical Image Computing and Computer Assisted Intervention–MICCAI 2020: 23rd International Conference, Lima, Peru, October 4–8, 2020, Proceedings, Part VII 23, pp. 657–666. Springer (2020)

117. Wang, Y., Luo, Y., Zu, C., Zhan, B., Jiao, Z., Wu, X., Zhou, J., Shen, D., Zhou, L.: 3d multi-modality transformer-gan for high-quality pet reconstruction. *Medical Image Analysis* **91**, 102983 (2024)
118. Wang, Y., Yu, B., Wang, L., Zu, C., Lalush, D.S., Lin, W., Wu, X., Zhou, J., Shen, D., Zhou, L.: 3d conditional generative adversarial networks for high-quality pet image estimation at low dose. *Neuroimage* **174**, 550–562 (2018)
119. Wang, Z., Bovik, A.C., Sheikh, H.R., Simoncelli, E.P.: Image quality assessment: from error visibility to structural similarity. *IEEE transactions on image processing* **13**(4), 600–612 (2004)
120. Wang, Z., Simoncelli, E.P., Bovik, A.C.: Multiscale structural similarity for image quality assessment. In: *The Thirty-Seventh Asilomar Conference on Signals, Systems & Computers*, 2003, vol. 2, pp. 1398–1402. IEEE (2003)
121. Wei, W., Poirion, E., Bodini, B., Durrleman, S., Ayache, N., Stankoff, B., Colliot, O.: Predicting pet-derived demyelination from multimodal mri using sketcher-refiner adversarial training for multiple sclerosis. *Medical image analysis* **58**, 101546 (2019)
122. Wen, Y., Chen, L., Deng, Y., Zhou, C.: Rethinking pre-training on medical imaging. *Journal of Visual Communication and Image Representation* **78**, 103145 (2021)
123. Wolleb, J., Bieder, F., Friedrich, P., Zhang, P., Durrer, A., Cattin, P.C.: Binary noise for binary tasks: Masked bernoulli diffusion for unsupervised anomaly detection. *arXiv preprint arXiv:2403.11667* (2024)
124. Wolleb, J., Bieder, F., Sandkühler, R., Cattin, P.C.: Diffusion models for medical anomaly detection. In: *International Conference on Medical image computing and computer-assisted intervention*, pp. 35–45. Springer (2022)
125. Wolleb, J., Sandkühler, R., Bieder, F., Valmaggia, P., Cattin, P.C.: Diffusion models for implicit image segmentation ensembles. In: *International Conference on Medical Imaging with Deep Learning*, pp. 1336–1348. PMLR (2022)
126. Wolterink, J.M., Leiner, T., Viergever, M.A., Išgum, I.: Generative adversarial networks for noise reduction in low-dose ct. *IEEE transactions on medical imaging* **36**(12), 2536–2545 (2017)
127. Wu, J., Fu, R., Fang, H., Zhang, Y., Yang, Y., Xiong, H., Liu, H., Xu, Y.: Medsegdiff: Medical image segmentation with diffusion probabilistic model. In: *Medical Imaging with Deep Learning*, pp. 1623–1639. PMLR (2024)
128. Xiao, Z., Kreis, K., Vahdat, A.: Tackling the generative learning trilemma with denoising diffusion gans. In: *International Conference on Learning Representations* (2021)
129. Xie, H., Gan, W., Zhou, B., Chen, X., Liu, Q., Guo, X., Guo, L., An, H., Kamilov, U.S., Wang, G., et al.: Dose-aware diffusion model for 3d ultra low-dose pet imaging. *arXiv preprint arXiv:2311.04248* (2023)
130. Xue, Y., Peng, Y., Bi, L., Feng, D., Kim, J.: Cg-3dsrgan: A classification guided 3d generative adversarial network for image quality recovery from low-dose pet images. In: *2023 45th Annual International Conference of the IEEE Engineering in Medicine & Biology Society (EMBC)*, pp. 1–4. IEEE (2023)
131. Ye, J., Ni, H., Jin, P., Huang, S.X., Xue, Y.: Synthetic augmentation with large-scale unconditional pre-training. In: *International Conference on Medical Image Computing and Computer-Assisted Intervention*, pp. 754–764. Springer (2023)
132. Yoon, J., Drumright, L.N., Van Der Schaar, M.: Anonymization through data synthesis using generative adversarial networks (ads-gan). *IEEE journal of biomedical and health informatics* **24**(8), 2378–2388 (2020)
133. Yoon, J.S., Zhang, C., Suk, H.I., Guo, J., Li, X.: Sadm: Sequence-aware diffusion model for longitudinal medical image generation. In: *International Conference on Information Processing in Medical Imaging*, pp. 388–400. Springer (2023)
134. Yu, F., Seff, A., Zhang, Y., Song, S., Funkhouser, T., Xiao, J.: Lsun: Construction of a large-scale image dataset using deep learning with humans in the loop. *arXiv preprint arXiv:1506.03365* (2015)

135. Zeng, P., Zhou, L., Zu, C., Zeng, X., Jiao, Z., Wu, X., Zhou, J., Shen, D., Wang, Y.: 3d cvt-gan: a 3d convolutional vision transformer-gan for pet reconstruction. In: International Conference on Medical Image Computing and Computer-Assisted Intervention, pp. 516–526. Springer (2022)
136. Zhang, J., He, X., Qing, L., Gao, F., Wang, B.: Bpgan: Brain pet synthesis from mri using generative adversarial network for multi-modal alzheimer’s disease diagnosis. *Computer Methods and Programs in Biomedicine* **217**, 106676 (2022)
137. Zhang, R., Isola, P., Efros, A.A., Shechtman, E., Wang, O.: The unreasonable effectiveness of deep features as a perceptual metric. In: Proceedings of the IEEE conference on computer vision and pattern recognition, pp. 586–595 (2018)
138. Zhao, P., Pan, H., Xia, S.: Mri-trans-gan: 3d mri cross-modality translation. In: 2021 40th Chinese Control Conference (CCC), pp. 7229–7234. IEEE (2021)
139. Zhu, L., Codella, N., Chen, D., Jin, Z., Yuan, L., Yu, L.: Generative enhancement for 3d medical images. arXiv preprint arXiv:2403.12852 (2024)
140. Zhu, L., Xue, Z., Jin, Z., Liu, X., He, J., Liu, Z., Yu, L.: Make-a-volume: Leveraging latent diffusion models for cross-modality 3d brain mri synthesis. In: International Conference on Medical Image Computing and Computer-Assisted Intervention, pp. 592–601. Springer (2023)
141. Zhu, Z., Tao, T., Tao, Y., Deng, H., Cai, X., Wu, G., Wang, K., Tang, H., Zhu, L., Gu, Z., et al.: Loci-diffcom: Longitudinal consistency-informed diffusion model for 3d infant brain image completion. arXiv preprint arXiv:2405.10691 (2024)